Supplement of Clim. Past, 15, 1275–1301, 2019
https://doi.org/10.5194/cp-15-1275-2019-supplement

Climate of the Past
Open Access
EGU

Supplement of

Combining a pollen and macrofossil synthesis with climate simulations for spatial reconstructions of European climate using Bayesian filtering

Nils Weitzel et al.

Correspondence to: Nils Weitzel (nweitzel@iup.uni-heidelberg.de)

1 Introduction

This supplement contains

- Pseudo-code for the MCMC and MC^3 algorithms used in the manuscript
- Additional figures from the identical twin experiments
- Results from spatial reconstructions with the other process stage models, that are not included in the Sect. 4.2 of the manuscript
- Additional figures from experiments with reduced proxy syntheses
- Results from sensitivity experiments with respect to the glasso penalty parameter ρ

2 Pseudo-code for MCMC algorithm

For our reconstructions, we run the MCMC algorithm for $J = 75,000$ iterations, discard the first $25,000$ as burn-in, and retain every fifth to reduce autocorrelation. This leads to $10,000$ posterior samples that are used for subsequent analyses. Pseudo-code for the MCMC algorithm is provided in Algorithm 1. If the modularized version is used, 75,000 samples of the transfer function parameters θ are drawn first. These are used for subsequent reconstructions.

Algorithm 1 Pseudo-code for MCMC algorithm

```
Initialize MCMC chain
for j = 1, ..., N do
    if TF Modus = 'FULL' then
        for T ∈ T(P) do
            for l = 1, ..., L(T) do
                Sample from full conditional of γ_l^T
            end for
            Sample from full condition of β^T
        end for
    else if TF Modus = 'MODULARIZED' then
        Load j-th sample of β^T
    end if
    if Process stage formulation = RM then
        Update λ with random walk type Metropolis-Hastings sampler
    end if
    if Process stage formulation = KM then
        Sample from full conditional of ω
        Sample from full conditional of z
    end if
    if Covariance matrix = Shrinkage then
        Update τ with independent Metropolis-Hasting sampler
        Choose Σ_prior according to τ
    end if
    for x ∈ x_P do
        Update C_p(x) with random walk type Metropolis-Hastings sampler
    end for
end for
for i = 1, ..., N do
    Sample from full conditional of C_p(x_Q)
end for
```

3 Pseudo-code for MC^3 algorithm

The MC^3 algorithm is used for reconstructions with the KM to overcome the multi-modality of this model. For our reconstructions, we use $J = 2500$ loops of $M = 30$ iterations to draw altogether 75,000 samples from $A = 8$ MCMC chains. The MC^3 algorithm follows the pseudo-code in Algorithm 2.

Algorithm 2 Pseudo-code for MC^3 algorithm

Initialize A MCMC chains
for $j = 1, ..., J$ **do**
  for $a = 1, ..., (A-1)$ **do**
    Run M steps of chain a following the MCMC Algorithm 1 to update γ, β, ω, z, τ, and $C_p(x_P)$
  end for
  for $a = 1, ..., (A-1)$ **do**
    Calculate Metropolis-Hastings ratio r of chains a and $a+1$
    Swap chains a and $a+1$ with probability $p = \max(1, r)$
  end for
end for
for $i = 1, ..., JM$ **do**
  Sample from full conditional of $C_p(x_Q)$
end for

4 Additional figures for identical twin experiments

Plotted below are the grid box deviation from the reference climatologies, averaged over all ITEs with the same process stage model, and the coverage frequency of each grid box for 50% CIs. Again, the frequencies are calculated over all ITEs with the same process stage model.

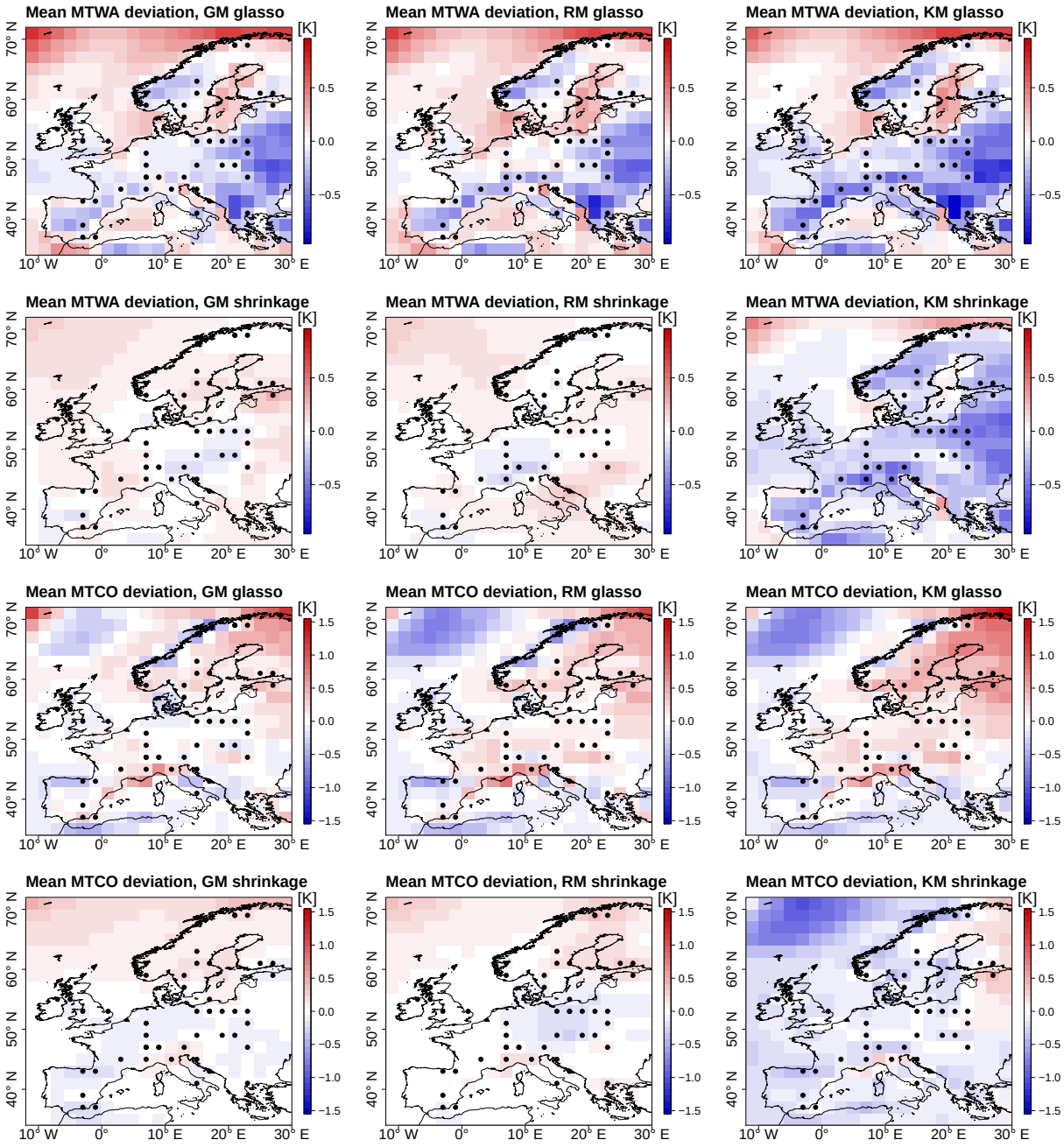

Figure 1. Mean deviation in identical twin esperiments for GM, RM, and KM. Top row: Models with glasso covariance matrix, MTWA. Second row: Models with shrinkage covariance matrix, MTWA. Third row: Models with glasso covariance matrix, MTCO. Bottom row: Models with shrinkage covariance matrix, MTCO. Grid boxes with proxy data are depicted by black dots.

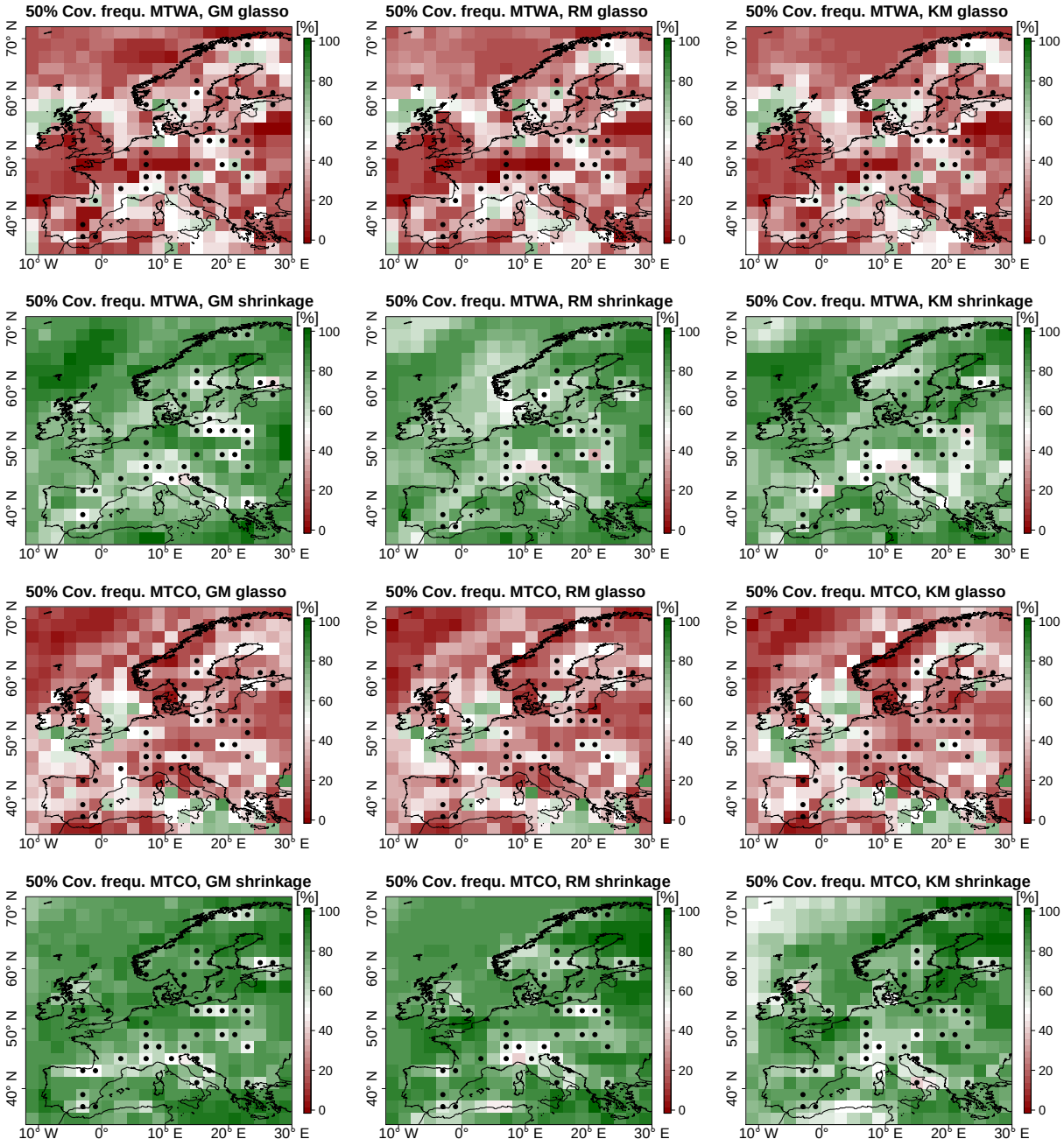

Figure 2. Coverage frequency for 50% credible intervals in identical twin esperiments for GM, RM, and KM. Target frequency is 50%. Top row: Models with glasso covariance matrix, MTWA. Second row: Models with shrinkage covariance matrix, MTWA. Third row: Models with glasso covariance matrix, MTCO. Bottom row: Models with shrinkage covariance matrix, MTCO. Grid boxes with proxy data are depicted by black dots.

5 Results from spatial reconstructions with alternative process stage models

In Sect. 4.2 of the manuscript, we only presented results with the RM using the shrinkage covariance matrix approach. In this Section, we provide results from spatial reconstructions of European MH climate with the other five process stage models, which where described in Sect. 3.3 and compared in Sect. 4.1 using ITEs and CVEs. Summary measures are given in Table 1. Figures 3 to 8 show results of the different experiments.

Similar to the ITEs, the choice of covariance matrix impacts the reconstruction more than using a different process stage formulation, i.e. GM, RM or KM.

The three reconstructions with shrinkage matrix have very similar estimates of the spatially averaged mean MTWA anomaly and the spatial structures are in very good agreement. For most of the domain, the posterior mean structure is also very similar for MTCO, but differences are found in the north-western part of the domain, that is least constrained by proxy data. Therefore, this is the region that is most affected by the different process stage formulations. Here, the KM is warmer than the RM, while the GM is cooler than the RM. This can be explained by the RM being the most flexible of the three such that the GM is more pulled towards the ensemble mean while the KM is pulled towards the MPI-ESM-P climatology, which is the favoured model. On the other, hand the RM departs from the ensemble mean towards the MPI-ESM-P climatology but not as strong as in the KM. The difference in the northern-western part of the domain is carried over to the spatially averaged mean MTCO anomaly which is lower in the GM reconstruction than in the RM one, but higher in the KM reconstruction than the RM one. The spatially averaged CI sizes as well as the spatial uncertainty pattern are in very good agreement between the three reconstructions. The spatial smoothness of the posteriors measured by the spatial homogeneity H (see Sect. 4.2.1 of the manuscript) is very similar between the three reconstructions.

Similarly, the three reconstruction with glasso covariance matrices are very similar, but differ in some regards from the shrinkage based reconstructions. The MTWA reconstruction is cooler in all three models, while the MTCO is warmer in all experiments. This is an effect of the stronger interaction between MTWA and MTCO in the glasso covariance matrices, as the shrinkage target Φ does not contain correlations between MTWA and MTCO. The spatial mean patterns tend towards more extreme values in the glasso than in the shrinkage based reconstructions. This can be explained by the fewer spatial modes in the glasso covariances, that lead to less robust reconstructions. The uncertainty estimates are significantly smaller than in the reconstructions with shrinkage covariances, due to the fewer spatial modes in the covariance matrix. This fits with the diagnosed under-dispersiveness of the glasso models in ITEs (see Sect. 4.1.1). The difference in the uncertainty estimates is larger for MTCO than MTWA, because the stronger inter-variable interaction in the glasso covariance matrices leads to a stronger uncertainty reduction compared to the unconstrained process stages in those three reconstructions. This also leads to a higher degree of spatial smoothing in the glasso based reconstructions for MTCO, while the estimates for MTWA are very similar to the reconstructions with shrinkage covariances.

All reconstructions with the RM as well as the KM favour the MPI-ESM-P climatology, which has the highest posterior weights in all those reconstruction. In the KM reconstruction, particle filter degeneracy, which is discussed in the manuscript as a major issue of the KM, can be diagnosed as the MPI-ESM-P climatology is chosen in more than 98% of MCMC samples.

Table 1. Summary measures for the joint MTWA and MTCO reconstructions with the five alternative process stage formulations. Numbers in brackets are minima and maxima of the corresponding 90% CIs. Provided are the spatially averaged posterior mean anomaly from the CRU reference climatology for MTWA and MTCO, the spatially averaged 90% CI sizes for MTWA and MTCO, the spatial homogeneity for MTWA and MTCO, and the PMIP3 ensemble member with the highest posterior weight, where applicable.

Reconstruction name	Mean anomaly MTWA	Mean anomaly MTCO	Mean 90% CI size MTWA	Mean 90% CI size MTCO	Spatial homogeneity MTWA	Spatial homogeneity MTCO	PMIP3 model with highest weight
GM shrinkage	(0.04 K) 0.53 K (1.02 K)	(-0.05 K) 0.55 K (1.14 K)	4.10 K	5.64 K	(1.29 K) 1.41 K (1.53 K)	(2.28 K) 2.53 K (2.75 K)	—
KM shrinkage	(0.02 K) 0.48 K (0.97 K)	(0.37 K) 0.92 K (1.51 K)	4.08 K	5.75 K	(1.31 K) 1.42 K (1.53 K)	(2.28 K) 2.50 K (2.69 K)	MPI-ESM-P
GM glasso	(-0.29 K) 0.05 K (0.36 K)	(0.66 K) 1.01 K (1.38 K)	2.89 K	3.15 K	(1.38 K) 1.45 K (1.53 K)	(2.08 K) 2.18 K (2.27 K)	—
RM glasso	(-0.31 K) 0.03 K (0.34 K)	(0.63 K) 1.02 K (1.37 K)	2.91 K	3.17 K	(1.38 K) 1.46 K (1.53 K)	(2.09 K) 2.17 K (2.27 K)	MPI-ESM-P
KM glasso	(-0.32 K) 0.01 K (0.33 K)	(0.74 K) 1.11 K (1.50 K)	2.90 K	3.18 K	(1.40 K) 1.48 K (1.57 K)	(2.09 K) 2.18 K (2.27 K)	MPI-ESM-P

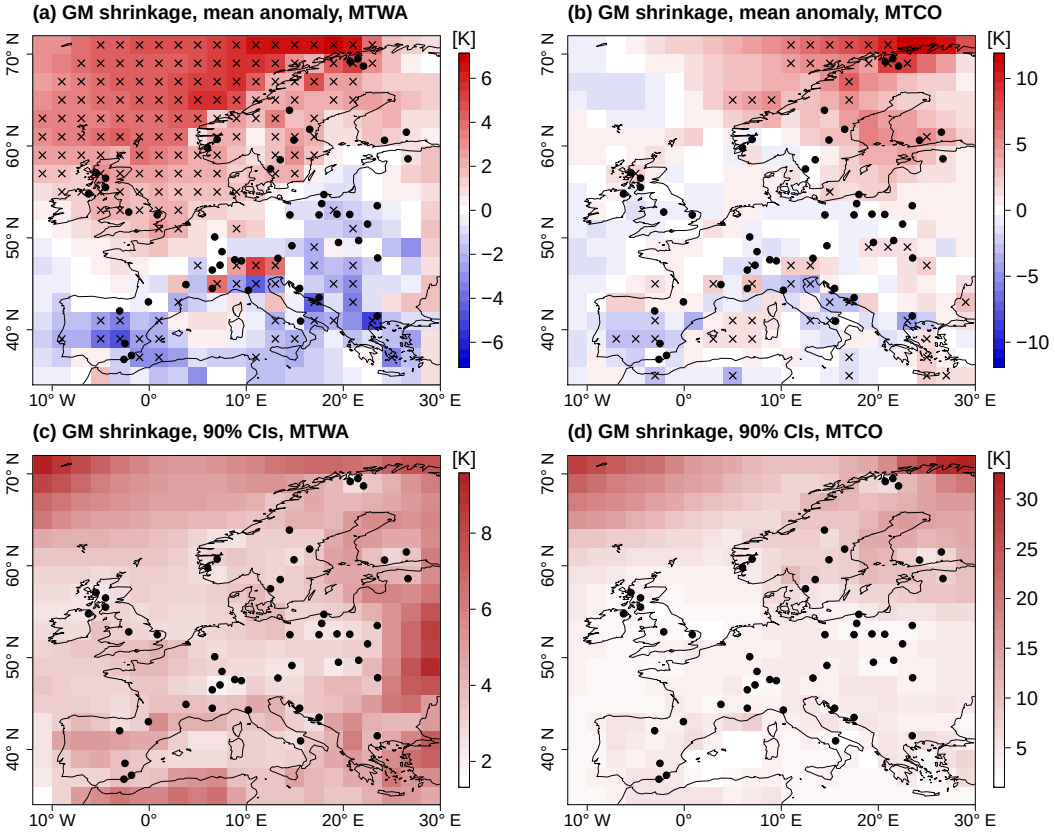

Figure 3. Spatial reconstruction for MH with the GM using the shrinkage covariance matrix. Top row: Posterior mean anomaly from CRU reference climatology (left: MTWA, right: MTCO), bottom row: reconstruction uncertainty plotted as size of point-wise 90% CIs (left: MTWA, right: MTCO). Black dots depict proxy samples. In the top row, point-wise significant anomalies (5% level) are marked by black crosses.

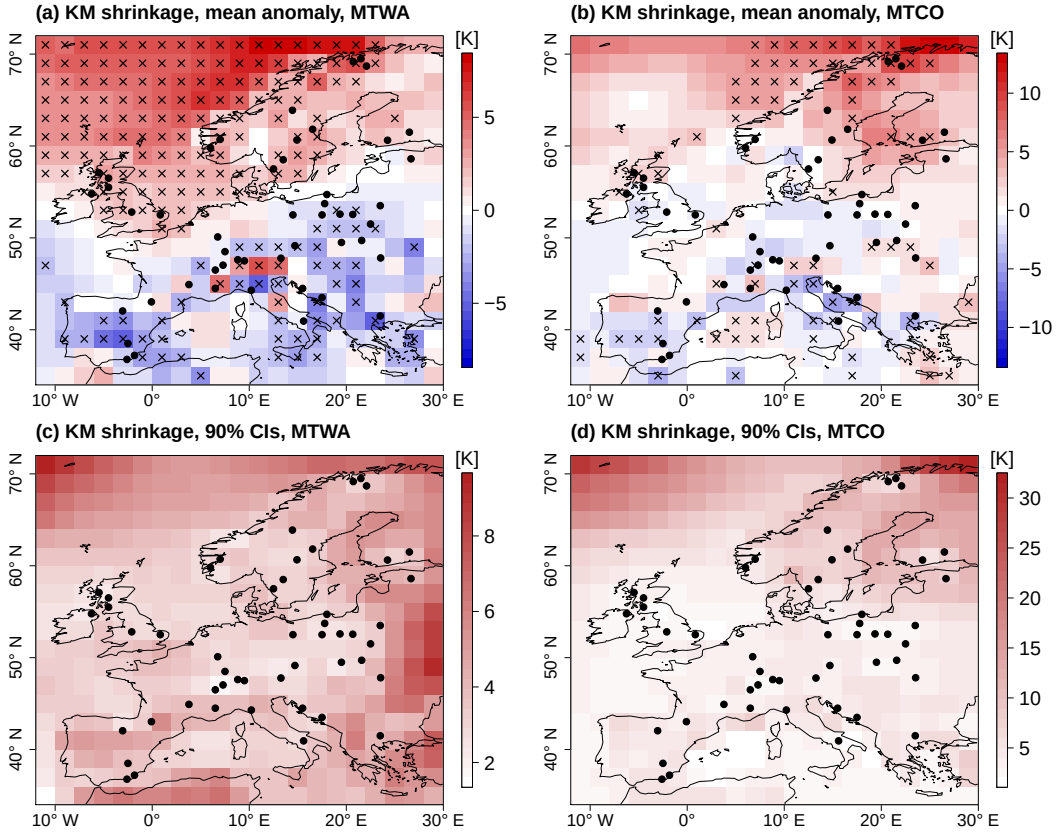

Figure 4. Spatial reconstruction for MH with the KM using the shrinkage covariance matrix. Top row: Posterior mean anomaly from CRU reference climatology (left: MTWA, right: MTCO), bottom row: reconstruction uncertainty plotted as size of point-wise 90% CIs (left: MTWA, right: MTCO). Black dots depict proxy samples. In the top row, point-wise significant anomalies (5% level) are marked by black crosses.

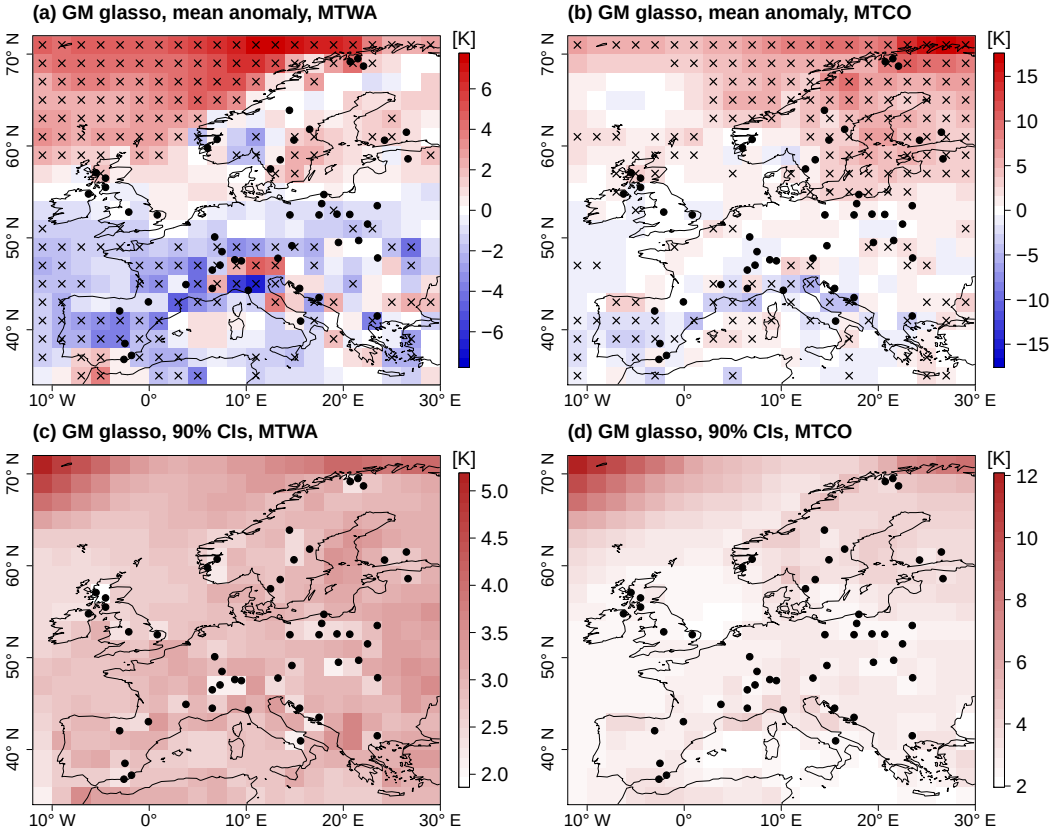

Figure 5. Spatial reconstruction for MH with the GM using the glasso covariance matrix. Top row: Posterior mean anomaly from CRU reference climatology (left: MTWA, right: MTCO), bottom row: reconstruction uncertainty plotted as size of point-wise 90% CIs (left: MTWA, right: MTCO). Black dots depict proxy samples. In the top row, point-wise significant anomalies (5% level) are marked by black crosses.

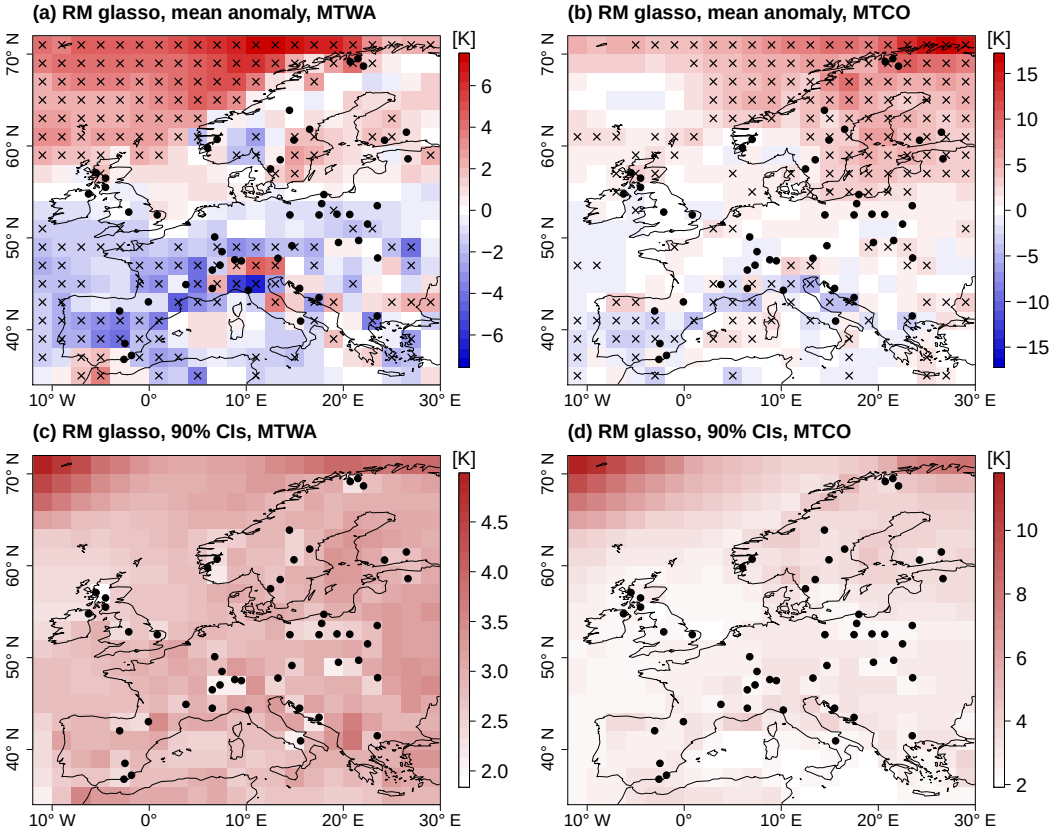

Figure 6. Spatial reconstruction for MH with the RM using the glasso covariance matrix. Top row: Posterior mean anomaly from CRU reference climatology (left: MTWA, right: MTCO), bottom row: reconstruction uncertainty plotted as size of point-wise 90% CIs (left: MTWA, right: MTCO). Black dots depict proxy samples. In the top row, point-wise significant anomalies (5% level) are marked by black crosses.

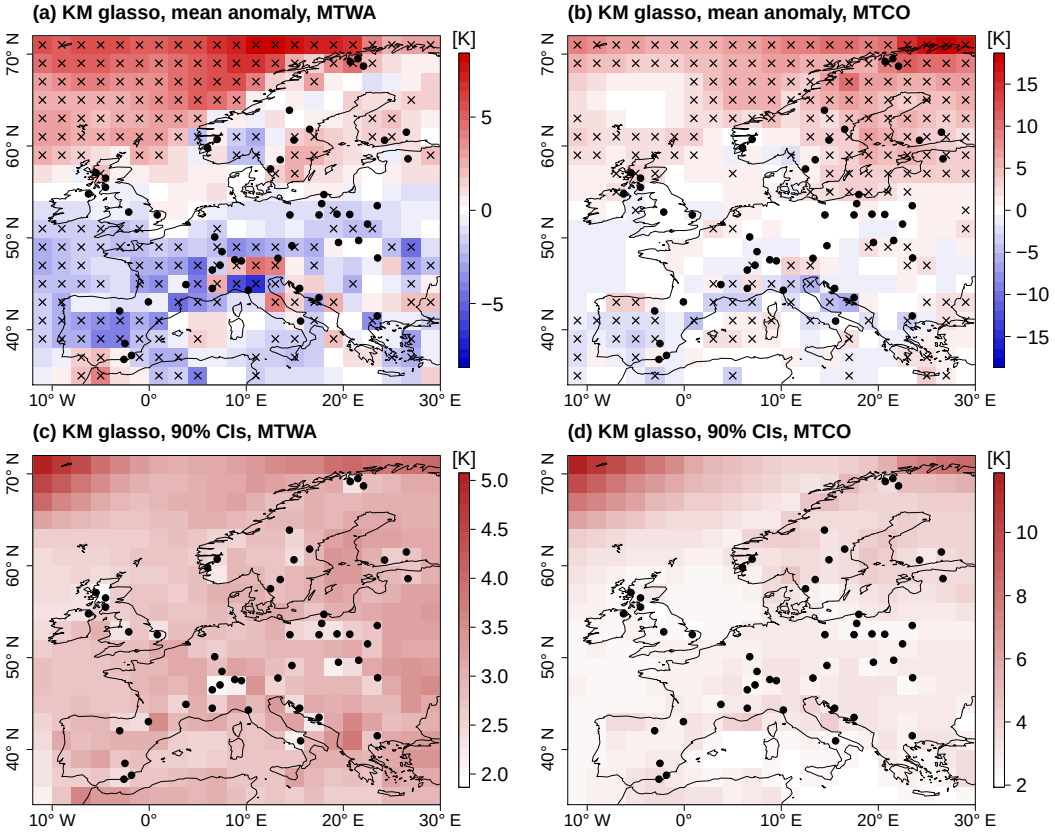

Figure 7. Spatial reconstruction for MH with the KM using the glasso covariance matrix. Top row: Posterior mean anomaly from CRU reference climatology (left: MTWA, right: MTCO), bottom row: reconstruction uncertainty plotted as size of point-wise 90% CIs (left: MTWA, right: MTCO). Black dots depict proxy samples. In the top row, point-wise significant anomalies (5% level) are marked by black crosses.

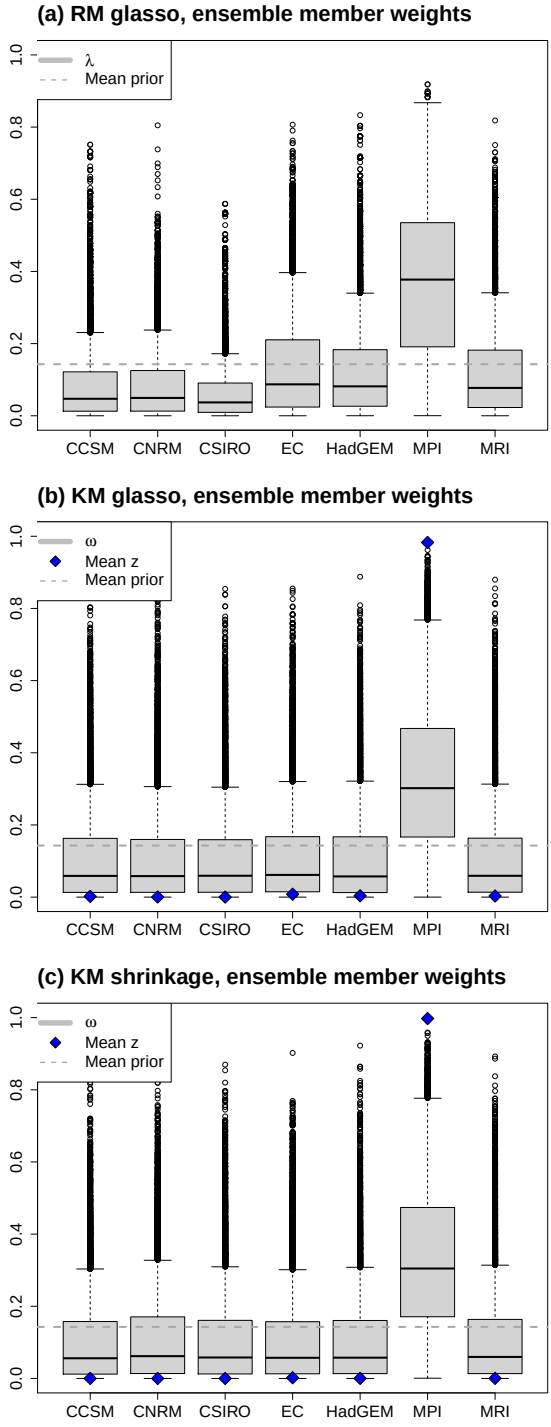

Figure 8. Posterior ensemble member weights of the reconstructions with RM glasso, KM glasso, and KM shrinkage. The mean of prior weights is denoted by the dashed line.

6 Sensitivity of reconstruction results with respect to the glasso penalty parameter

As described in Sect. 3.3 of the manuscript, the glasso algorithm, which regularizes the covariance matrix estimated from the PMIP3 ensemble, requires the specification of a penalty parameter ρ. Values of at least 0.3 produce numerically stable matrices. Larger values lead to smaller correlations, and therefore higher posterior uncertainties due to less spatial transfer of information from the proxy data. To test the influence of ρ on the reconstruction results, we compute reconstructions and cross-validations with the RM for $\rho = 0.3, 0.5, 0.7, 1.0, 2.0$.

The fraction of the penalty term on the total cost given by Eq. (14) increases from 79.5% for $\rho = 0.3$ to 98.5% for $\rho = 2.0$ (Fig. 9) showing the generally high influence of the penalty term due to the small ensemble size and the increasing importance for larger ρ. While the mean BS is lowest for $\rho = 0.3$ with 0.37 and increases with ρ, the differences are small in total with 0.44 being the highest value for $\rho = 2.0$ (Fig. 9). The mean value of the posterior climate and the posterior ensemble member weights are insensitive to changes in ρ with differences in the mean spatial average of less than 0.2 K (Fig. 9) as well as no substantial regional differences, and mean λ values which differ less than 0.06 for each of the ESM climatologies. On the other hand, the posterior uncertainty grows substantially for larger ρ values. While the spatially averaged size of point-wise 90% CIs is 3.04 K for $\rho = 0.3$, the value increases to 6.41 K for $\rho = 2.0$ (Fig. 9).

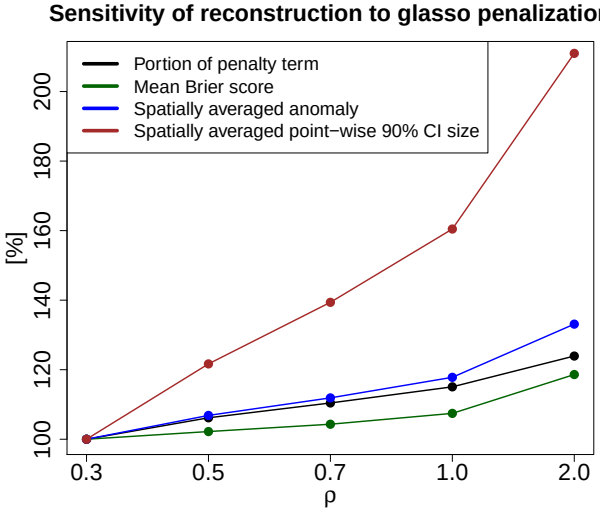

Figure 9. Sensitivity of reconstructions to changes in the glasso penalty parameter ρ. Portion of the penalty term on the total cost in Eq. (14), mean BS of cross-validations, spatially averaged posterior mean anomaly from CRU reference climatology, and spatially averaged size of point-wise 90% CIs. All quantities are plotted as percentage of the respective values for $\rho = 0.3$. Note the non-linear scaling of the x-axis.

7 Figures from experiments with reduced proxy dataset

In Sect. 5.1, results from reconstructions with a reduced proxy dataset were discussed. In each of those five experiments, half of the proxy samples are removed from the synthesis, and a reconstruction is computed with the remaining records. Here, we provide plots corresponding to each of the reconstructions, numbered by Experiment 1 to Experiment 5. For each experiment, we plot the posterior mean anomaly for MTWA and MTCO, the size of 90% CIs for MTWA and MTCO, and the posterior ensemble member weights λ.

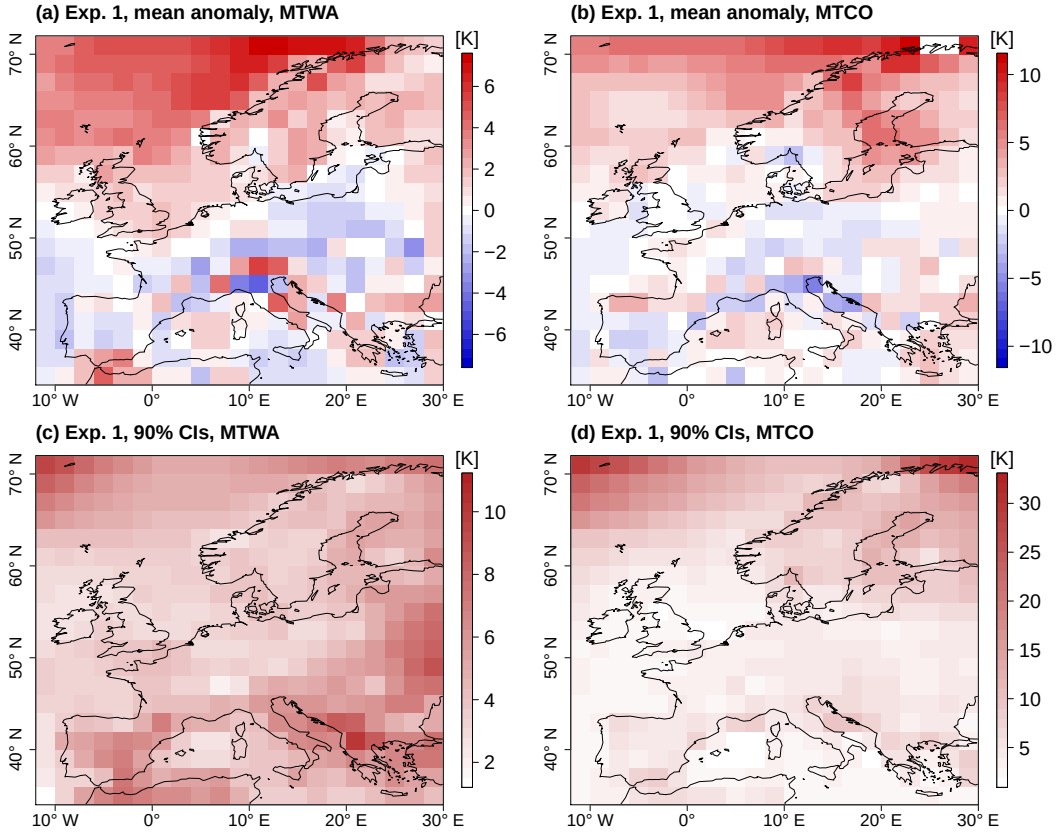

Figure 10. Reduced data experiment 1. Top row: Posterior mean anomaly from CRU reference climatology (left: MTWA, right: MTCO), bottom row: reconstruction uncertainty plotted as size of point-wise 90% CIs (left: MTWA, right: MTCO).

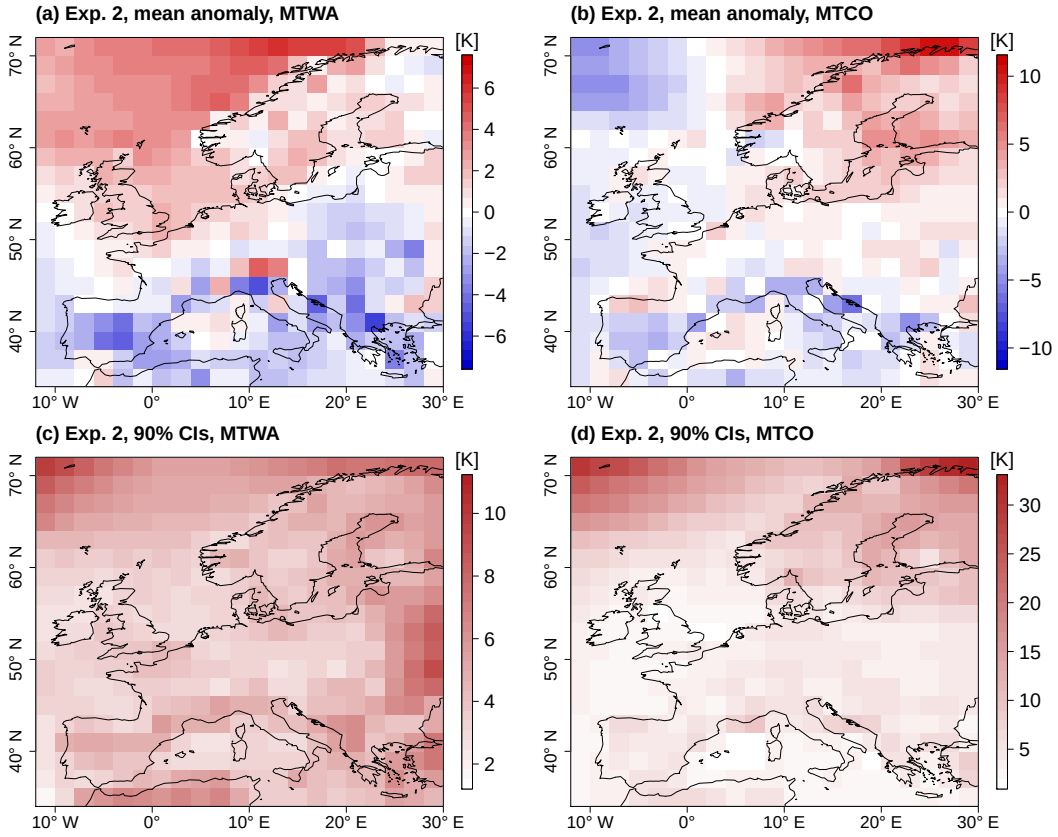

Figure 11. Reduced data experiment 2. Top row: Posterior mean anomaly from CRU reference climatology (left: MTWA, right: MTCO), bottom row: reconstruction uncertainty plotted as size of point-wise 90% CIs (left: MTWA, right: MTCO).

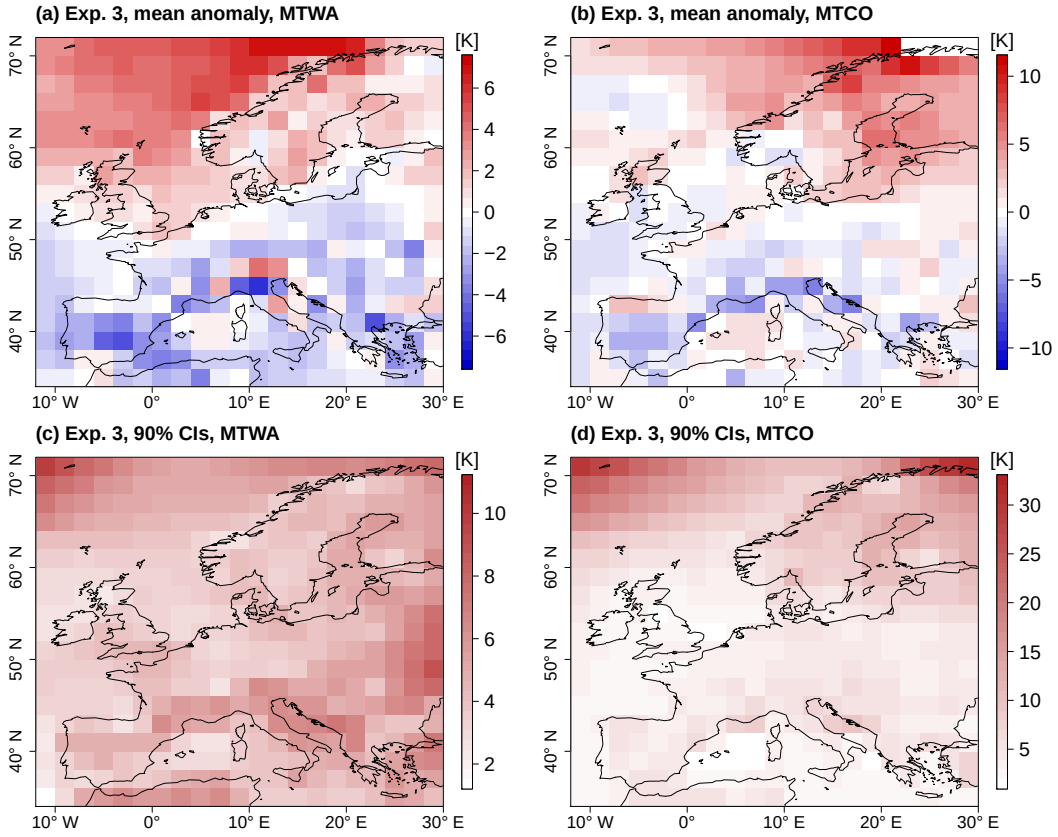

Figure 12. Reduced data experiment 3. Top row: Posterior mean anomaly from CRU reference climatology (left: MTWA, right: MTCO), bottom row: reconstruction uncertainty plotted as size of point-wise 90% CIs (left: MTWA, right: MTCO).

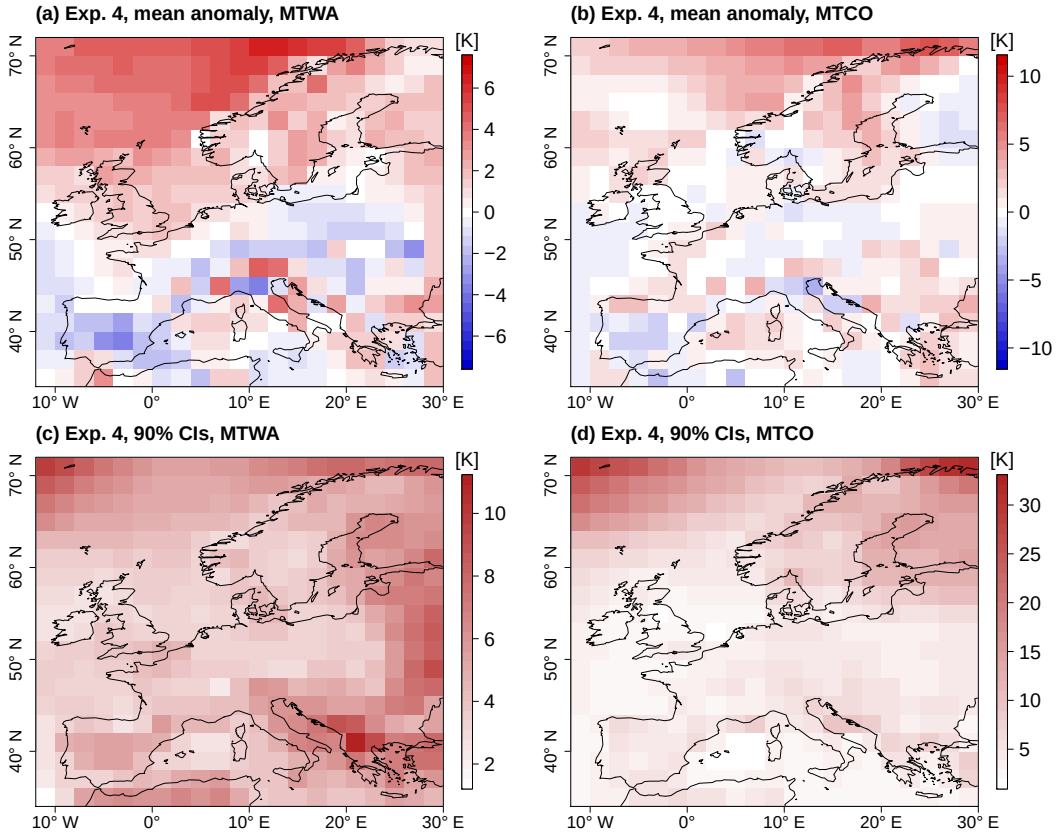

Figure 13. Reduced data experiment 4. Top row: Posterior mean anomaly from CRU reference climatology (left: MTWA, right: MTCO), bottom row: reconstruction uncertainty plotted as size of point-wise 90% CIs (left: MTWA, right: MTCO).

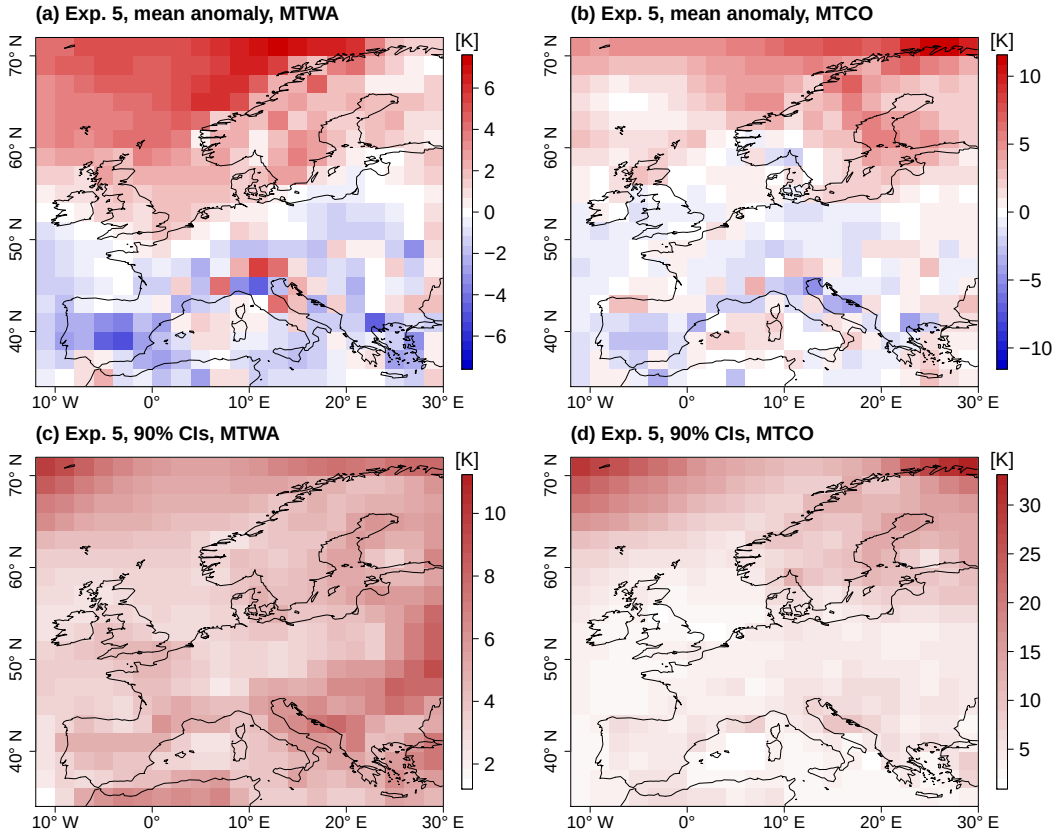

Figure 14. Reduced data experiment 5. Top row: Posterior mean anomaly from CRU reference climatology (left: MTWA, right: MTCO), bottom row: reconstruction uncertainty plotted as size of point-wise 90% CIs (left: MTWA, right: MTCO).

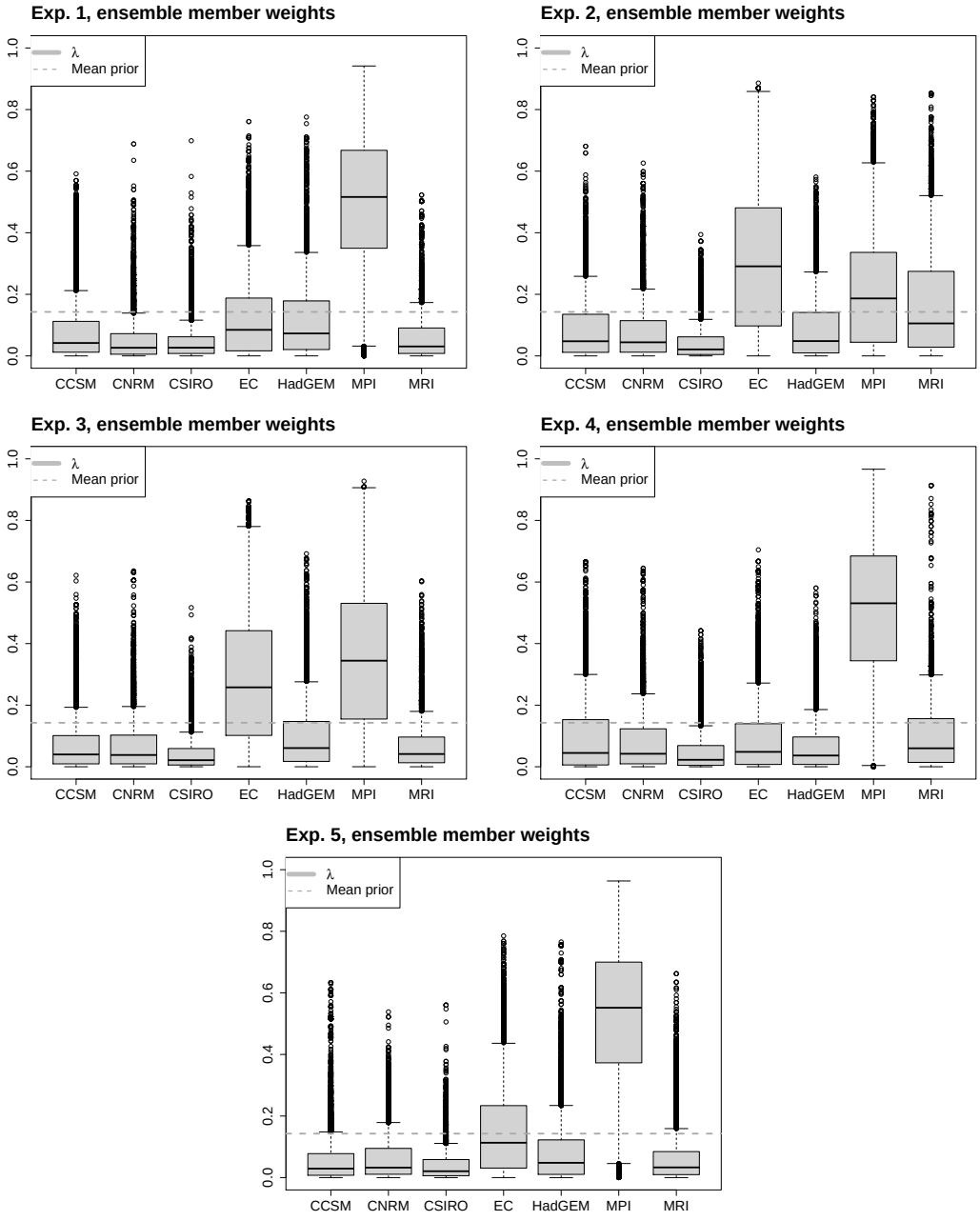

Figure 15. Posterior ensemble member weights of the five experiments with reduced proxy syntheses. The mean of prior weights is denoted by the dashed line.